substance: boron compounds with group IV elements: boron carbide
property: electronic properties

Electron density distribution in boron carbide $B_{13}C_2$ (cubic BN and TiB_2) [86W3].

band structure calculations

The structural formula of boron carbide is $(B_{12})_x(B_{11}C)_{1-x}(CBC)_m(CBB)_n(CCC)_o(B\square B)_p$ (m+n+o+p = 1; for $B_{4.3}C$ o, p = 0). All the hitherto performed band structure calculation on boron carbide are based on the assumption of idealized structures for well-defined chemical compositions. That means that one specific hypothetical arrangement of atoms in a well-defined unit cell is occasionally assumed. However, as shown above, the real structure consists of a statistical arrangement of differently structured elementary cells. In any case, their individual concentration is too high to allow the assumption of a small perturbation of one of them. For example in the least-disturbed structure at the carbon-rich limit of the homogeneity range there are 100 % $B_{11}C$ icosahedra and 82% CBC and 18% CBB chains. The composition $B_{13}C_2$, which has often been assumed to be the ideal boron carbide, is in reality the mostly distorted structure in the whole homogeneity range and contains about 60% $B_{11}C$ icosahedra, 40% B_{12} icosahedra, 64% CBC chains, 18% CBB chains and 18% chainless cells.

Band structure calculations yield insulating/semiconducting character for $B_{12}C_3$ (structure formula $B_{11}C(CBC)$) and metallic character for $B_{13}C_2$ (structure formula $B_{12}(CBC)$) (see e.g. [95L]). It is important that these calculations are based on the experimentally determined real atom positions. This means that the Jahn-Teller effect, which has been assumed to be responsible for the semiconducting character of the icosahedral boron-rich solids (see e.g. [90W1] and LB III/41C) is implicitly considered in these calculations.

Recent investigations [98S, 99S1] suggest that the high concentration of defects could play an essential role for the electronic properties of the icosahedral boron-rich solids, if the experimentally determined deviations from certain idealized structures are taken into account. Atoms in interstitial sites of boron carbide can be largely excluded, therefore such defects are in particular: (i) exchange of B and C atoms in sites in icosahedra or chains, (ii) vacancies in chainless unit cells. Since – apart from the different number of electrons – the valence structures of B and C are approximately equal, in a first approximation the exchange of these atoms is expected to evoke donor or acceptor levels in the band gap. If for example $B_{13}C_2$ ($B_{12}(CBC)$) is taken as the ideal structure, the formation of 50 % $B_{11}C(CBB)$ by C-B exchange would exactly compensate the electron deficiency in the valence band by the formation of one donor and one acceptor state per C-B exchange. The incomplete compensation according to the experimentally determined concentration of structure elements can be compensated by the chainless unit cells (for details see [98S, 99S2]).

Ab-initio band structure calculations for the hypothetical structures $B_{11}C(CBC)$ and $B_{12}(CBC)$ in Fig. 1 [90B1, 91B, 91K].

Other results of energy band structure calculation of $B_{12}(CBC)$ and $B_{11}C(CBC)$ in Fig. 2 [95L]. For the resulting densities of states see Fig. 3.

General discussion of band structure calculations of boron-rich solids [87A].

Electronic band structure calculation of $B_{12}C_3$ also in [89H]. For previous band structure calculations of $B_{12}C_3$ see [81A1, 83A1]. The valence band structure exhibits a series of flat, non-free-electron-like bands, with little variation in energy for any one band throughout the *k*-space (Fig. 4). According to these calculations the Fermi level is expected within the valence band near its upper limit (Figs. 4, 5). The metallic behavior expected according to these calculations does not agree with the experimental results which are available at present. Besides, the calculated band gap of about 2.5 eV disagrees with the experiments (cf. [71W, 74W, 81W1]).

para-carborane ($p\text{-}C_2B_{10}H_{12}$) as a system for the study of structure and interaction in carbon-containing icosahedra [87B].

Electronic studies of different hypothetical compositions of the structural elements in boron carbide in Fig. 6. Conclusion: One C in the icosahedron is highly favored over 0,2, or 3; the CBC chain is highly favored over all other chains [91F].

Discussion of the general influence of the Jahn-Teller effect on the electronic properties in [90W1] (see also LB III/41C "Boron").

calculated cohesive energies of different assumed structures of boron carbide
(in eV)

$E(B_{12}(CBC)$	7.1408	91B12,
$E(B_{11}C(BBC)_{\alpha}$	7.0013	90B1,
$E(B_{11}C(BBC)_{\beta}$	6.9926	93B
$E(B_{11}C(BBC)_{\gamma}$	6.9482	
$E(B_{12}(BBC)$	6.9312	
$E(B_{11}C(CBC)$	7.2592	
$E(B_{12})$	6.8402	
E(C)	8.3895	

calculated energy reduction in charged icosahedra
(E in eV)

B_{12} icosahedron

E	~ 3.7	total for 2 electrons added	87H2
	~ 2.7	from electron filling	
	~ 1.0	from contraction of the icosahedron by ~ 0.09 Å	

$B_{11}C$ icosahedron

E	~ 18.2	total for 2 electrons added	87H2
	~ 16.5	from electron filling	
	~ 1.7	from contraction of the icosahedron by ~ 0.09 Å	

calculated Mulliken effective charge
(in e)

q	3.024	B(1)	hypothetical $B_{13}C_2$	95L
	3.04(2)	B(1)’	hypothetical $B_{13}C_2$	
	2.874	B(2)	hypothetical $B_{13}C_2$	
	2.92(2)	B(2)’	hypothetical $B_{13}C_2$	
	2.20(1)	B(3)	hypothetical $B_{13}C_2$	
	4.66(2)	(C)	hypothetical $B_{13}C_2$	
	3.21(2)	B(1)	hypothetical $B_{11}C$(CBC)	
	3.14(2)	B(1)’	hypothetical $B_{11}C$(CBC)	
	2.98(1)	B(1)’’	hypothetical $B_{11}C$(CBC)	
	2.75(2)	B(2)	hypothetical $B_{11}C$(CBC)	
	2.22(2)	B(2)’	hypothetical $B_{11}C$(CBC)	
	2.83(1)	B(2)’’	hypothetical $B_{11}C$(CBC)	
	2.78(1)	B(2)’’’	hypothetical $B_{11}C$(CBC)	
	2.26(1)	B(3)	hypothetical $B_{11}C$(CBC)	
	4.28(1)	(C)	hypothetical $B_{11}C$(CBC)	
	4.53(1)	(C)’	hypothetical $B_{11}C$(CBC)	
	4.50(1)	(C)’’	hypothetical $B_{11}C$(CBC)	

From these results was concluded in [87H2] that the assumed charge transport in boron carbide by bipolarons in $B_{11}C$ icosahedra is strongly energetically favored over that via B_{12} icosahedra. This is in contrast to the experimental result that the maximum electrical conductivity coincides with the maximum concentration of B_{12} icosahedra (see below).

density of states

The electronic structure of crystalline boron carbide; selfconsistent calculation energy eigenvalues, density of states, and valence electron distributions for hypothetical boron carbide of the idealized composition $B_{13}C_2$ (polar and equatorial atoms in the B_{12} icosahedra and C-B-C chains separately), B_{12} icosahedra without chains and chains without icosahedra, s-like and p-like states in Fig. 7 [90S].

Total and partial density of states determined with the first-principles orthogonalized linear combination of atomic orbitals method in Fig. 3 [95L].

Further density of states calculations in [82B, 83A1, 84A, 90B2, 91B, 94B, 86B].

Density of states experimentally determined from dc electrical conductivity and from dynamical conductivity compared with the density of B_{12} icosahedra in Fig. 8 [97S, 98W].

Optically determined density of states of a C level in β-rhombohedral boron and in boron carbide in [90W2].

charge densities

Partial s- and p-like charges (in *e*) for the nonequivalent positions of the model crystals B_{12}(BCB), B_{12}(CBC) and B_{12}(CCC) (α-rhombohedral B for comparison) [97R].

	B_{12}(CBC)		B_{12}(BCB)		B_{12}(CCC)		α-rh. B	
Position	s	p	s	p	s	p	s	p
B(1)	0.296	0.645	0.309	0.658	0.292	0.650	0.286	0.576
B(2)	0.299	0.629	0.304	0.631	0.297	0.638	0.295	0.264
chain B	0.385	0.556	0.331	0.731	-	-	-	-
chain C	0.598	1.366	0.727	1.116	0.641 [a])	1.076 [a])	-	-
					0.551 [b])	1.229 [b])		

[a]) central position in the chain, [b]) end position in the chain.

Contours of constant charge densities in the surface of the $B_{11}C$ icosahedron in Fig. 9 [90B10]; for contours in the surface of the B_{12} icosahedron see [91B].

Deformation of the electron densities through one of the bisecting planes of the icosahedron $B_{4.3}C$ in [87H1].

Electron density calculations for the top triangle of a B_{12} icosahedron and a plane perpendicular to the *c axis* in [91F].

experimental

XANES spectrum in Fig. 10 [98M].

Auger electron spectroscopy of B_4C and B_9C boron carbide in Fig. 11 [86M].

energy gaps
(in eV)

calculated:

E_g	2.915	indirect, calculated for $B_{13}C_2$ (hypothetical structure $B_{11}C$(CBC))	91K
	3.116	direct, calculated for $B_{13}C_2$	
	2.781	indirect, calculated for $B_{12}C_3$ (hypothetical structure B_{12}C(CCC))	
	3.050	direct, calculated for $B_{12}C_3$	
	3.01	A →A ($B_{13}C_2$), Z → A B_{11}C(CBC) (calc)	95L
	3.48	Γ (calculated)	
	4.14	X (calculated)	
	3.48	Z (calculated)	
	3.01	A (calculated)	
	3.01	D (calculated)	

experimental:				
E_g	0.18	T = 300 K	transition energies obtained	92W
	0.47		from optical absorption	
	0.77			
	0.92			
	1.20			
	2.01			
	2.17			
	2.97			
	3.16			
	3.41			
	3.58			
	3.94			
	4.13			
	4.67			
	4.85			
	5.81			
	6.00			
	0.065	low T	derived from spin density [96C]	98S,
			and Hall density [91W2]	99S1
	0.068		electrical conductivity (see Fig. 12)	86W2
	0.13			
	0.46			
$E_{g,ind}$	0.48 eV	T = 300K	optical absorption (see Fig. 13)	71W, 74W
	> 4 eV		calculated	81A1, 83A1
	0.5...1 eV		calculated (tight binding approximation)	57Y

The chemical composition of the samples can be assumed to be close to the carbon-rich limit of the homogeneity range $B_{4.3}C$.

photoluminescence energies
(uncertain value in parantheses)
(E in eV)

E	1.563	T = 290 K	$B_{4.23}C$, recombination of free excitons	99S2
	1.572			
	(1.552)			

Photoluminescence spectrum in Fig. 14 [99S2].

activation energy for conductivity
(in eV)

E_A	0.166	T = 380...590 K	p = 0	85S
	0.176		p = 9.94 kbar	
	0.193		p = 19.40 kbar	

The chemical composition of the samples can be assumed to be close to the carbon-rich limit of the homogeneity range $B_{4.3}C$.

Preliminary band scheme of boron carbide in Fig. 15 [98S, 99S1].

Dependence of activation energy of the electrical conductivity on the composition Fig. 16 [86W1, 86W2, 86W4, 91W1].

Temperature dependence of the activation energy of the el. cond. of single crystals in [90W1] (see Fig. 17).
Rutherford backscattering spectrum in [91R] (see Fig. 18 (comparison with N-implanted boron carbide).

Interband critical points

Boron carbide, minima of the 2nd derivatives of ε_1 and ε_2 in eV. Type of critical points estimated from the 1st derivative, energy of the critical points E_{crit} (in eV) estimated according to the typical position relative to the 2nd derivative minima (example: derivative spectra of ε_1 and ε_2 of $^{10}B_{4.3}C$ in Fig. 19 [97W].

$B_{4.3}$ C(+C)		**$^{10}B_{4.3}$ C**		**$B_{4.23}$ C**		**$B_{4.51}$ C**		**$B_{4.66}$ C**		**$B_{6.28}$ C**		**$B_{6.4}$ C**		**$B_{8.52}$ C**		**$B_{10.37}$ C**		**$^{10}B_{4.3}$ C**	
ε_1	ε_2	ε_1	ε_2	ε_1	ε_2	ε_1	ε_2	ε_1	ε_2	ε_1	ε_2	ε_1	ε_2	ε_1	ε_2	ε_1	ε_2	Type	E_{crit}
	2.7		2.625		2.625						2.7				2.625		2.625	M1	
3.0	3.35	2.99	3.325	3.05	3.33	3.0	3.425	2.875	3.425	3.0	3.5	2.975	3.425	2.925	3.325	3.025	3.325	M1	3.2
3.75	4.0	3.8	3.975	3.75	4.025	3.725		3.725		3.725		3.9		3.75	3.975	3.7	4.075	M0	3.7
4.175	4.45	4.175	4.35	4.125	4.46	4.15	4.3	4.1	4.3	4.15			4.575	4.125	4.35	4.125	4.45	M1	4.3
4.55	4.775	4.65	4.68	4.675	4.9	4.525		4.525	4.825	4.675	4.825	4.8		4.625	5.0			M1	4.8
4.975	5.375	5.0	5.025	5.15	5.5	4.975	5.45	4.95	5.425		5.4		5.475	5.0	5.5		5.525	M1	5.0
5.675	5.775	5.625	5.75	5.625		5.45		5.6		5.375		5.525		5.5	5.725			M0	5.6
		5.875	6.0															M2(?)	5.9
6.275	6.65	6.375	6.675	6.4	6.475	6.0	6.475	6.25	6.45	6.25	6.425	6.325	6.525	6.2	6.725	6.4	6.5	M1	6.5
6.875	7.375	7.02	7.1	6.975	7.5	6.675		6.725		7.075			7.075	7.275	7.35	7.05	7.225	M1	7.1
		7.275	7.425															M1(?)	7.3
7.7	7.875	7.65	7.8	7.425	7.8	7.6	7.325	7.825	7.325	7.575	7.65	7.7		7.675	7.8	7.62	7.575	M2	7.9
	8.275	8.175	8.175	7.9		8.025				8.1			8.175	8.125	8.15	8.175	8.35	M1	8.2
8.525	8.675	8.45	8.525	8.525	8.625	8.575	8.525	8.325	8.525		8.575			8.575	8.675	8.7	8.75	M3	8.5
9.2		9.15	9.15	9.025		8.975		8.8		8.7		8.675	8.725	9.0		9.175		M0	9.1

critical points in the interband transition range
(obtained from structure-modulated reflectivity spectra)
(in eV)

	$^{10}B_{4.3}C$	$^{nat}B_{4.51}C$	$^{nat}B_{10.37}C$	
E_{crit}	1.398	1.398	1.41	99W
	1.50	1.51	1.57	
	2.51	2.50	2.51	
	2.72	2.70	2.72	
	3.18	3.18	3.20	
	3.88	3.92	3.93	
	4.08	4.14	4.20	
	4.85	4.80	4.88	

***g*-values**

(7.2% C)				
g	2.0028(3)	T = 300 K	ΔH_{max} = 5.3 Oe, asymm. A/B ~1.9	80V
	2.0038(3)	T = 77 K	ΔH_{max} = 6.2 Oe, asymm. A/B ~0.66	
	2.0038(3)	T = 4.2 K	ΔH_{max} = 12.6 Oe, asymm. A/B ~1.2	
(16 % C; 300 K and 77 K no signal)				
g	2.0032(3)	T = 4.2 K	ΔH_{max} = 5.3 Oe, asymm. A/B ~1.5	
$g_{\perp}$	2.0039	T = 4.2 K	ΔH = 10 Oe	
$g_{\parallel}$	2.004			
(22 % C)				
g	2.0029	T = 300 K	ΔH_{max} = 4.5 Oe, symm almost Lorentzian	80V
	2.0033	T = 77 K	ΔH_{max} = 9.1 Oe, symm almost Lorentzian	
	2.0035	T = 4.2 K	ΔH_{max} = 18.0 Oe, Lorentzian	

***g*-values** (± 10.0002 mostly) and **line widths** ΔB ($\cdot 10^{-4}$ T) of the single, isotropic, symmetrical EPR line in boron carbide [77G]

	single crystal		polycrystal		powder, powder + 5 wt% C		crystalline, also with Be	
	[64G]		[64G, 70G]		[70K1]		[70K2]	
T[K]	g	ΔB	g	ΔB	g	ΔB	g	ΔB
1.7	2.0030	14	2.0035	10	–	–	–	–
77	–	5	2.001	8	–	4	–	6
300	–	8	2.000		2.0032	9	2.0030 (asymp.)	–

For EPR investigation on various boron-carbon compounds, see [68K1, 68K2].

spin density
(in spins/g)

n_S	$2.5 \cdot 10^{19}$	$T < 100$ K	B_4C	86V
	$1.8 \cdot 10^{19}$		$B_{13}C_2$	
	$3.6 \cdot 10^{19}$		$B_{15}C_2$	
	$3.2 \cdot 10^{19}$		B_9C	
	10^{20}	$T = 6$ K	largely independent of composition, temp.dep. Curie like	91D

ESR spectrum of boron carbide with 18 at.% C at 150 K in Fig. 20 [96C].

Spin density, susceptibility, g-factor and linewidth of boron carbide with high carbon concentration (> 19 at.%) for 4…1200 K in Fig. 21 [96C].

Spin density (T = 4...300 K) compared with Hall density of boron carbide with 18.2 and 16% C, respectively, in Fig. 22 [96C].

Spin density of $B_{4.3}C$ [96C] with fit [98S] compared with the Hall density [90W3] in Fig. 23 [98S, 99S1].

Temperature dependence of magnetic susceptibility and ESR linewidth of boron carbide with 18,16, 13 and 10 at.% C in Fig. 24 [96C].

Temperature dependence of the ESR linewidth compared with the temperature dependence of the Hall mobility below 300 K for boron carbide with 16 and 18.2 at.% C in Fig. 25 [96C].

Detailed discussion and review of earlier ESR measurements of different authors, ESR study of hot-pressed boron carbide, spectra of B_4C and $B_{12}C_3$ at2, 50, 300 K.; temperature dependence of the ESR spin susceptibility vs. T in Fig. 26 [87V, partly also in 86V], angle dependence of the ESR linewidth at 4 K for a single crystal and a ceramic sample in Fig. 27 [87V].

EPR investigation in [80V]: ESR intensity, linewidth and electrical resistivity depending on C content in Fig. 28 (abscissa is correctly in wt. % C) [80V].

effective hole mass

m_p	~10 m_0		estimated from band structure calc.	83A2
	5...10 m_0	$T = 300$ K	estimated from different exp. results	98S
	~10 m_0	$T = 290$ K	estimated from photoluminescence	99S2

Figures

Brillouin zone: Fig. 29, band structure: Fig. 4, total density of states: Fig. 5, electron paramagnetic resonance: Fig. 28; valence electron density distribution: Fig. 30; position of Fermi level: Fig. 31; density of states and hopping energy: Fig. 32

References:

57Y Yamazaki, M.: J. Chem. Phys. 27 (1957) 746.

64G Geist, D.: Int. Conf. Phys. Semicond., Paris (M. Hulin, ed.) 1964 p. 767.

68K1 Kollmann, J. J., Perol, N., Taglang, P.: C. R. Acad. Sci. (Paris) B 267 (1968) 15.

68K2 Kollmann, J. J., Taglang, P.: C. R. Acad. Sci. (Paris) B 266 (1968) 759.

70E Boron 3, T. Niemyski, ed., PWN Warsaw, 1970

70G Geist, D., Meyer, J., Peußner, H.: see [70E] p. 207.

70K1 Koulmann, J. J., Kappel, H., Taglang, P.: C. R. Acad. Sci. (Paris) 270 B (1970) 445.

70K2 Khusidman, M. B., Neshpor, V. S.: Poroshk. Metall. 9 (1970) 67.

71A Armstrong, D. R., Perkins, P. G., Stewart, J. J. P.: J. Chem. Soc. Sect. A (1971) 3674.

71W Werheit, H., Binnenbruck, H., Hausen, A.: Phys. Status Solidi (b) 47 (1971) 153.

74K Korsukova, M. M., Gurin, V. N., Sorokin, V. N., Yusov, Yu. P., Terent'eva, S. P., in: Bor, Poluchenie, Struktura i Svoistva, Ed.: Tavadze F. N., Moscow Nauka, 1974, p. 235.

74W Werheit, H., Binnenbruck, H.: see [74K], p. 110.

76A Armstrong, D. R., Breeze, A., Perkins, P. G.: J. Phys. C 8 (1976) 3558.

77A Armstrong, D. R., Breeze, A., Perkins, P. G.: J. Chem. Soc. Faraday Trans. II 73 (1977) 952.

77B Berezin, A. A., Golikova, O. A., Zaitsev, V. R., Kazanin, M. M., Orlov, V. M., Tkalenko, E. N., in:Boron and Refractory Borides, (Matkovich V. 1., ed.) Springer: Berlin, Heidelberg, New York 1977, p. 52.

77G Geist, D.: see [77B], p. 65.

79K1 Kirfel, A., Gupta, A., Will, G.: Acta Crystallogr. B 35 (1979) 1052.

79K2 Kirfel, A., Gupta, A., Will, G.: Acta Crystallogr. B 35 (1979) 2291.

80V Vlasova, M. V., Kakazey, N. G., Kosolapova, T. Y., Makarenko, G. N., Marek, F. V., Uskokovic, D., Risuc, M. M.: J. Mater. Sci. 15 (1980) 1041.

80W1 Werheit, H., de Groot, K.: Phys. Status Solidi (b) 97 (1980) 229.

80W2 Weill, G., Smirnov, I.A., Gurin, V.N.: J. Phys. (France) Colloq. 41, C5 (1980) 185.

81Al Armstrong, D. R.: Proc. 7th Int. Symp. Boron, Borides and Related Compounds. Uppsala, Sweden, 1981; spec. issue of J. Less-Common Met. 82 (1981) 357.

81A2 Armstrong, D. R., Bolland, J., Perkins, P. G. (abstract only): [81A1], p. 358.

81W1 Werheit, H., de Groot, K., Malkemper, W., Lundström, T.: see [81A1], p. 163.

81W2 Werheit, H., de Groot, K., Malkemper, W.: see [81A1], p. 153.

82B Bullett, D.W.: J. Phys.C: Solid State 15 (1982) 415.

83A1 Armstrong, D.R., Bolland, J., Perkins, P.G., Will, G., Kirfel, A.: Acta Crystallogr. B39 (1983) 324.

83A2 Armstrong, R., Bolland, J., Perkins, P.G., Will, G., Kirfel, A.: Acta Crystallogr. B 39 (1983) 1487.

84A Armstrong, D.R., Bolland, J., Perkins, P.G.: Theor. Chim. Acta 64 (1984) 501.

85S Samara, G.A., Emin, D., Wood, C.: Phys. Rev. B 32 (1985) 2315.

86B Bullett, D.W.: in: Boron-Rich Solids (AIP Conf. Proc. 140), Albuquerque, New Mexico 1985, D. Emin, T.L. Aselage, C.L. Beckel, I.A. Howard ed., American Institute of Physics: New York, 1986, p. 249.

86M Madden, H.H., Nelson, G.C., Wallace, W.O.: in: Boron-Rich Solids (AIP Conf. Proc. 140), Albuquerque, New Mexico 1985, D. Emin, T.L. Aselage, C.L. Beckel, I.A. Howard ed., American Institute of Physics: New York, 1986, p. 121.

86V Venturini, E.L., Azevedo, L.J., Emin, D., Wood, C.: in: Boron-Rich Solids (AIP Conf. Proc. 140), Albuquerque, New Mexico 1985, D. Emin, T.L. Aselage, C.L. Beckel, I.A. Howard ed., American Institute of Physics: New York, 1986, p. 292.

86W1 Wood, C.: in: Boron-Rich Solids (AIP Conf. Proc. 140), Albuquerque, New Mexico 1985, D. Emin, T.L. Aselage, C.L. Beckel, I.A. Howard ed., American Institute of Physics: New York, 1986, p. 206.

86W2 Werheit, H., Franz, R., Higashi, I.: J. Less-Common Met. 117 (1986) 169 (Proc. 8th Int. Symp. Boron, Borides, Carbides, Nitrides and Rel. Compounds, Tbilisi, Oct. 8 - 12, 1984).

86W3 Will, G., Kirfel, A.: in: Boron-Rich Solids (AIP Conf. Proc. 140), Albuquerque, New Mexico 1985, D. Emin, T.L. Aselage, C.L. Beckel, I.A. Howard ed., American Institute of Physics: New York, 1986, p. 87.

86W4 Wood, C.: in: Boron-Rich Solids (AIP Conf. Proc. 140), Albuquerque, New Mexico 1985, D. Emin, T.L. Aselage, C.L. Beckel, I.A. Howard ed., American Institute of Physics: New York, 1986, p. 362.

87A Armstrong, D.R.: in: Proc. 9th Int. Symp. Boron, Borides and Rel. Compounds, University of Duisburg, Germany, Sept. 21 - 25, 1987, H. Werheit ed., University of Duisburg: Duisburg, 1987, p. 125.

87B Beckel, C.L., Obarski, G.E., Fuka, M.Z., Fritts, J.D.: in: Novel Refractory Semiconductors, MRS Symp. Proc. Vol. 97, D. Emin, T.L. Aselage, C. Wood ed., Materials Research Soc.: Pittsburgh, 1987, p. 95.

87H1 Higashi, I., Ito, T.: in: Proc. 9th Int. Symp. Boron, Borides and Rel. Compounds, University of Duisburg, Germany, Sept. 21 - 25, 1987, H. Werheit ed., University of Duisburg: Duisburg, 1987, p. 41.

87H2 Howard, I.A., Beckel, C.L., Emin, D.: in: Novel Refractory Semiconductors, MRS Symp. Proc. Vol. 97, D. Emin, T.L. Aselage, C. Wood ed., Materials Research Soc.: Pittsburgh, 1987, p. 39.

87V Venturini, E.L., Emin, D., Aselage, T.L.: in: Novel Refractory Semiconductors, MRS Symp. Proc. Vol. 97, D. Emin, T.L. Aselage, C. Wood ed., Materials Research Soc.: Pittsburgh, 1987, p. 57.

89H Hatakeyama, T.: in: Electronic Structures of Icosahedral Boron Solids, University of Tokyo ed., Tokyo, 1989.

90B1 Bylander, D.M., Kleinman, L., Lee, S.: Phys. Rev. B 42 (1990) 1394.

90B2 Bullett, D.W.: in: The Physics and Chemistry of Carbides, Nitrides and Borides; NATO ASI Series E: Applied Sciences Vol. 185, R. Freer ed., Kluwer Academic Publishers: Dordrecht, 1990, p. 513.

90S Switendick, A.C.: in: The Physics and Chemistry of Carbides, Nitrides and Borides; NATO ASI Series E: Applied Sciences Vol. 185, R. Freer ed., Kluwer Academic Publishers: Dordrecht, 1990, p. 525.

90W1 Werheit, H.: in: The Physics and Chemistry of Carbides, Nitrides and Borides; NATO ASI Series E: Applied Sciences Vol. 185, R. Freer ed., Kluwer Academic Publishers: Dordrecht, 1990, p. 677.

90W2 Werheit, H.: in: The Physics and Chemistry of Carbides, Nitrides and Borides; NATO ASI Series E: Applied Sciences Vol. 185, R. Freer ed., Kluwer Academic Publishers: Dordrecht, 1990, p. 705.

90W3 Werheit, H., Herstell, B., Winkelbauer, W.: (unpublished results)).

91B Bullett, D.W.: AIP Conf. Proc. 231 (1991) 21, in: Boron-Rich Solids, Proc. 10th Int. Symp. Boron, Borides and Rel. Compounds, Albuquerque, NM 1990 (AIP Conf. Proc. 231), D. Emin, T.L. Aselage, A.C. Switendick, B. Morosin, C.L. Beckel ed., American Institute of Physics: New York, 1991, p. 21.

91D de Rooy, J.C.J.M., Reefman, D., van der Putten, D., Brom, H.B, Aselage, T., Emin, D.: in: Boron-Rich Solids, Proc. 10th Int. Symp. Boron, Borides and Rel. Compounds, Albuquerque, NM 1990 (AIP Conf. Proc. 231), D. Emin, T.L. Aselage, A.C. Switendick, B. Morosin, C.L. Beckel ed., American Institute of Physics: New York, 1991, p. 90.

91F Florence, M.M., Beckel, C.L.: in: Boron-Rich Solids, Proc. 10th Int. Symp. Boron, Borides and Rel. Compounds, Albuquerque, NM 1990 (AIP Conf. Proc. 231), D. Emin, T.L. Aselage, A.C. Switendick, B. Morosin, C.L. Beckel ed., American Institute of Physics: New York, 1991, p. 37.

91K Kleinman, L.: in: Boron-Rich Solids, Proc. 10th Int. Symp. Boron, Borides and Rel. Compounds, Albuquerque, NM 1990 (AIP Conf. Proc. 231), D. Emin, T.L. Aselage, A.C. Switendick, B. Morosin, C.L. Beckel ed., American Institute of Physics: New York, 1991, p. 13.

91R Reeber, R.R., Whitley, J.Q., Kusy, R.P., Culbertson, R.J., Yu, N.: in: Boron-Rich Solids, Proc. 10th Int. Symp. Boron, Borides and Rel. Compounds, Albuquerque, NM 1990 (AIP Conf. Proc. 231), D. Emin, T.L. Aselage, A.C. Switendick, B. Morosin, C.L. Beckel ed., American Institute of Physics: New York, 1991, p. 647.

91W1 Wang, Bo-Cheng, Chiu, Ying-Nan: Theochem 77 (1991) 1.

91W2 Werheit, H., Kuhlmann, U., Franz, R., Winkelbauer, W., Herstell, B., Fister, D., Neisius, H.: in: Boron-Rich Solids, Proc. 10th Int. Symp. Boron, Borides and Rel. Compounds, Albuquerque, NM 1990 (AIP Conf. Proc. 231), D. Emin, T.L. Aselage, A.C. Switendick, B. Morosin, C.L. Beckel ed., American Institute of Physics: New York, 1991, p. 104.

92W Werheit, H., Laux, M., Kuhlmann, U., Telle, R.: Phys. Status Solidi (b) 172 (1992) K81.

93B Bylander, D.M., Kleinman, L., Lee, S.: Phys. Rev. B 47 (1993) 10056.

94B Bullett, D.W.: Proc. 11th Int. Symp. Boron, Borides and Rel. Compounds, Tsukuba, Japan, August 22 - 26, 1993, Jpn. J. Appl. Phys. Series 10 (1994), p. 31.
95L Li, Dong, Ching, W.Y.: Phys. Rev . B 52 (1995) 17073.
96C Chauvet, O., Emin, D., Forro, L., Aselage, T.L., Zuppiroli, L.: Phys. Rev. B 53 (1996) 14450.
97L Lee, S.P., Kim, C.K., Nahm, K., Mittag, M., Jeong, Y.H., Ryu, C.M.: J. Appl. Phys. 81 (1997) 2454.
97R Ripplinger, H., Schwarz, K., Blaha, P.: J. Solid State Chem. 133 (1997) 51 (Proc. 12th Int. Symp. Boron, Borides and Rel. Compounds, Baden, Austria, 1996).
97S Schmechel, R., Werheit, H.: J. Solid State Chem. 133 (1997) 335 (Proc. 12th Int. Symp. Boron, Borides and Rel. Compounds, Baden, Austria, Aug. 25 - 30, 1996).
97W Werheit, H., Janowitz, C., Schmechel, R., Tanaka, T., Ishizawa, Y.: J. Solid State Chem. 133 (1997) 132 (Proc. 12th Int. Symp. Boron, Borides and Rel. Compounds, Baden, Austria, Aug. 25 - 30, 1996).
98M Meyer, F.D.: in: Thesis, Albert-Ludwigs-Universität Freiburg ed., Freiburg, Germany, 1998 .
98S Schmechel, R.: Thesis, Gerhard-Mercator University Duisburg, Germany, 1998.
98W Werheit, H.: in: Materials Science of Carbides, Nitrides and Borides (Proc. NATO ASI on "Materials science of carbides, nitrides and borides", St. Petersburg, Russia, August 12-22, 1998), Y.G. Gogotsi, R.A. Andrievski ed., Kluwer Academic Publishers, 1998, p. 65.
99S1 Schmechel, R., Werheit, H.: J. Phys.: Condens. Matter 11 (1999) 6803.
99S2 Schmechel, R., Werheit, H.: J. Phys.: Condens. Matter (1999) (submitted).
99W Werheit, H.: in: Electric Refractory Materials, Y. Kumashiro ed., Marcel Dekker: New York, 1999 (in press).

Fig. 1.

Boron carbide. Calculated energy bands of **(a)** hypothetical B_{12}(CBC) and **(b)** hypothetical $B_{11}C$(CBC). The dashed bands are odd under reflection and the solid ones even [90B1, 91B, 91K].

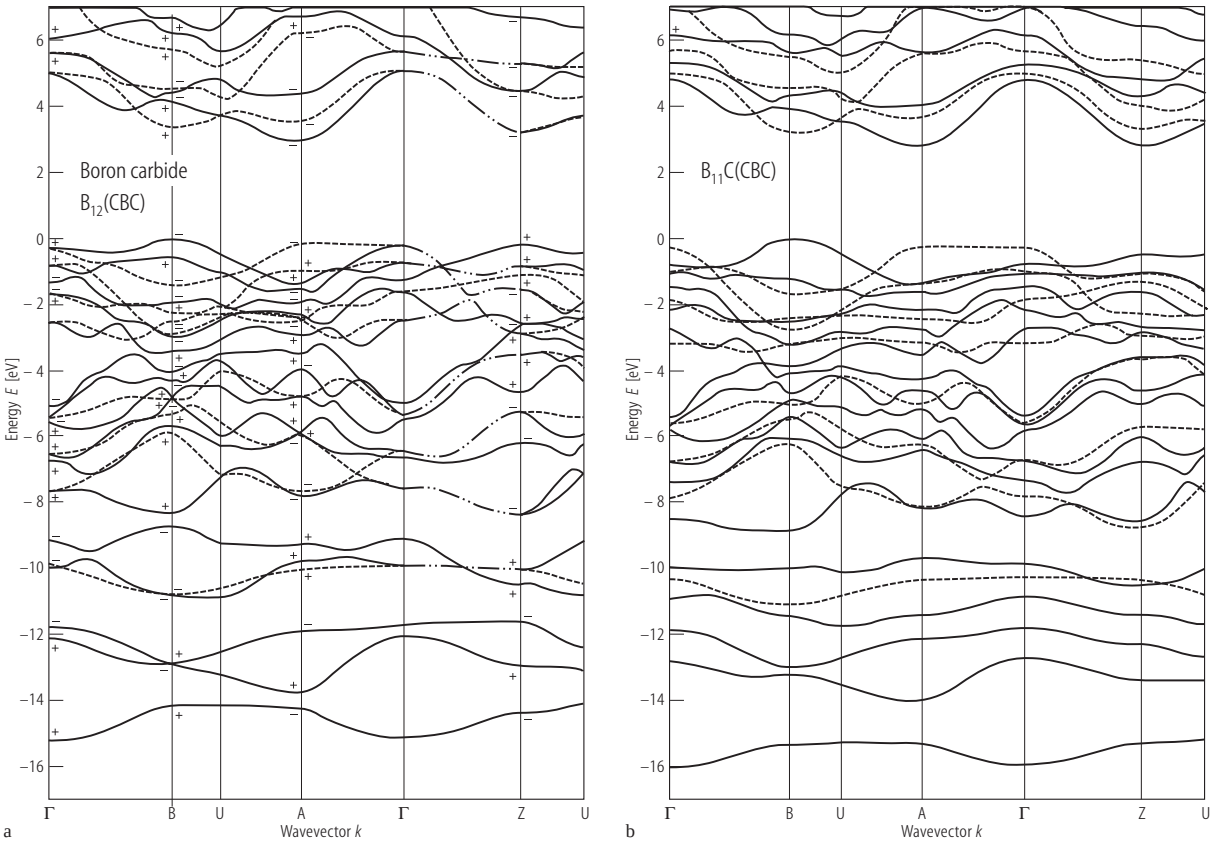

Fig. 2.

Boron carbide. Calculated energy bands of **(a)** hypothetical B_{12}(CBC) and **(b)** hypothetical $B_{11}C$(CBC) [95L].

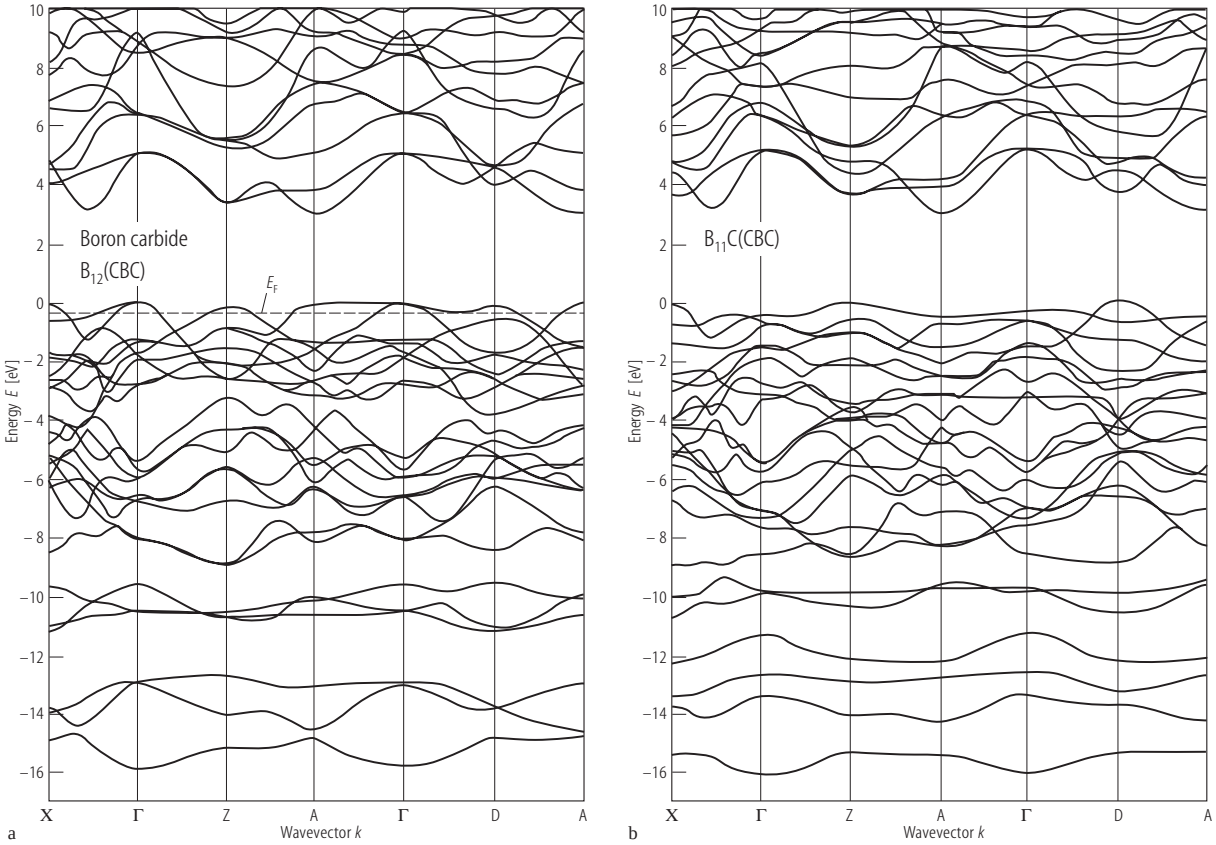

Fig. 3.

Boron carbide, hypothetical $B_{11}C(CBC)$. Total and partial densities of states vs. energy ($E_F = 0$). **(a1)** TDOS of $B_{11}C(CBC)$; **(a2)** TDOS of $B_{12}(CBC)$; **(b)** $B_{11}C(CBC)$: **(b1)** PDOS of icosahedral B, **(b2)** PDOS of chain B, **(b3)** PDOS of icosahedral C, **(b4)** PDOS of chain C; **(c)** $B_{12}(CBC)$: **(c1)** PDOS of icosahedral B, **(c2)** PDOS of chain B, **(c3)** PDOS of chain C [95L].

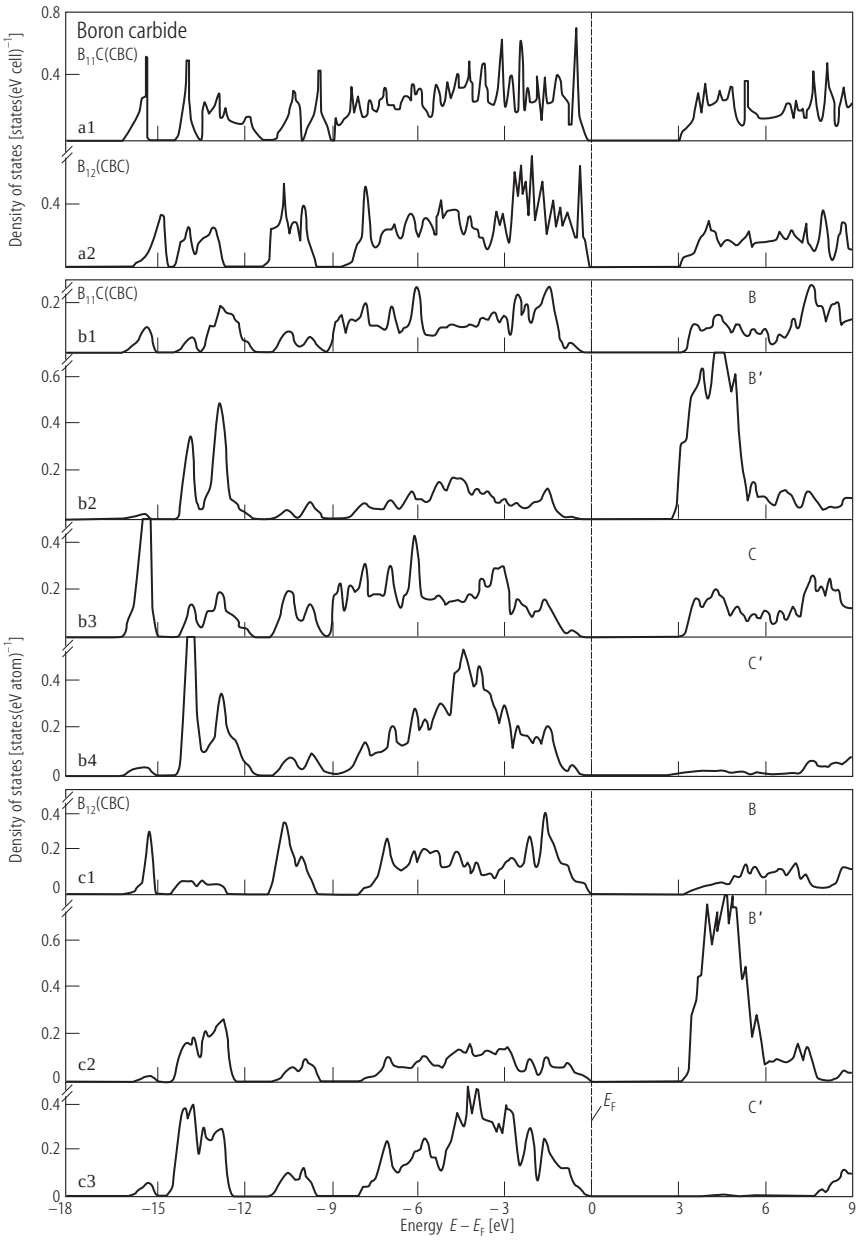

Fig. 4.

Boron carbide. Band structure for $B_{13}C_2$ [83A1, 81A2]. The calculations on $B_{13}C_2$ assumed a unit cell of that formula and this was allowed to interact with ca. 1000 neighboring unit cells. The input geometrical data and atomic data for the calculation were taken from [79K1] and [71A]. The calculational method (improved version of the SCMO-method) is fully described in [76A, 77A].

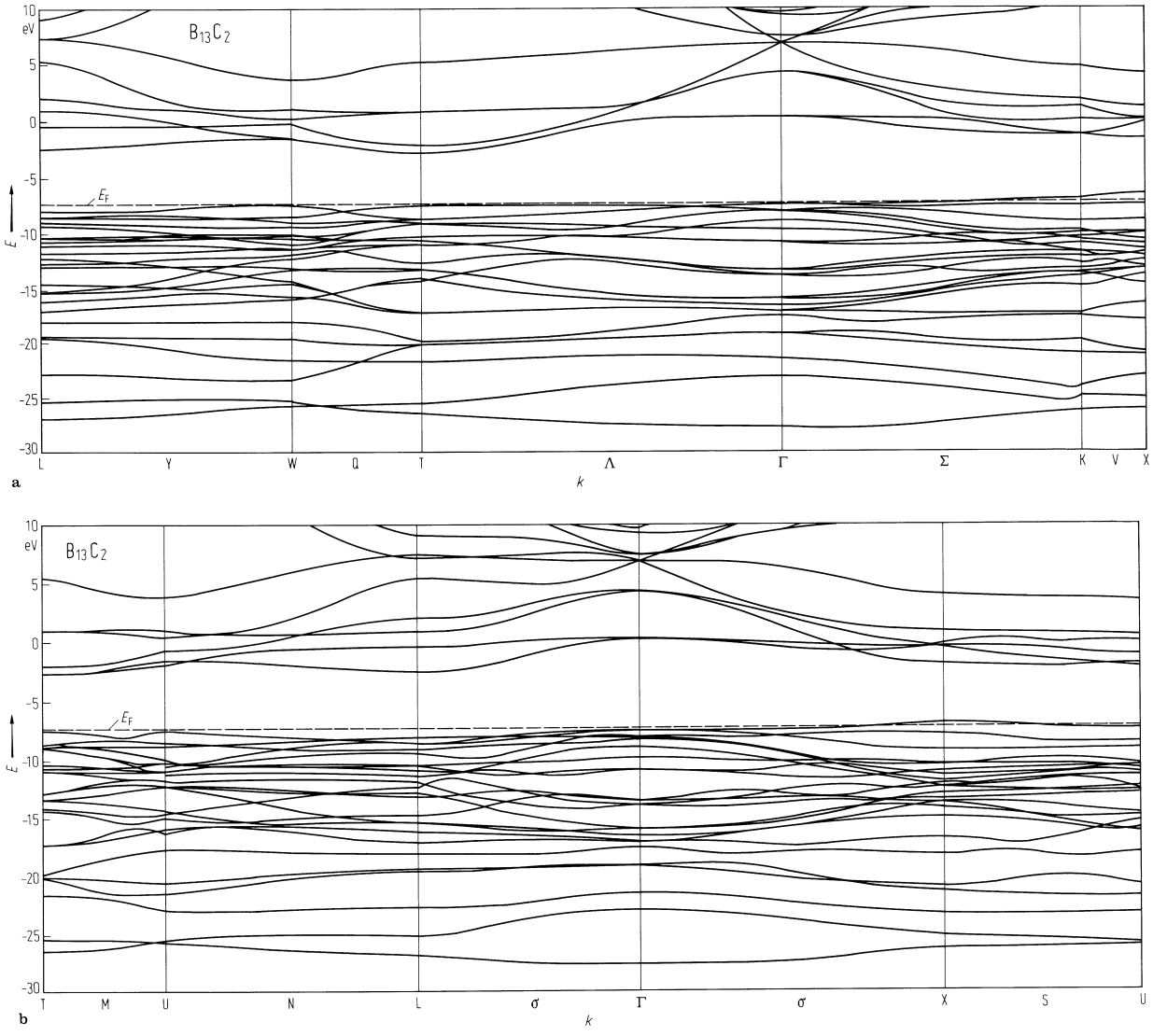

Fig. 5.

Boron carbide. Total electron density of states for $B_{13}C_2$ [81A2, 83A1].

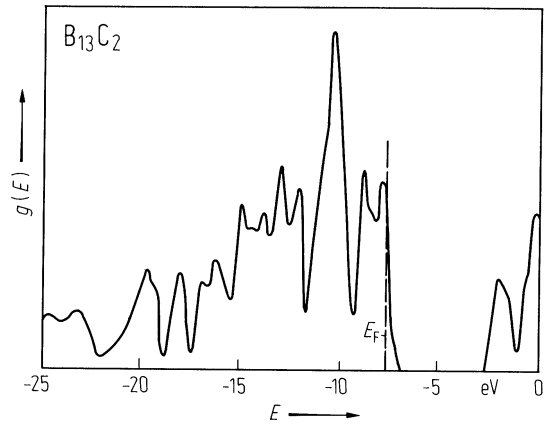

Fig. 6.

Boron carbide. Energies of tied-off icosahedral-chain clusters [91F].

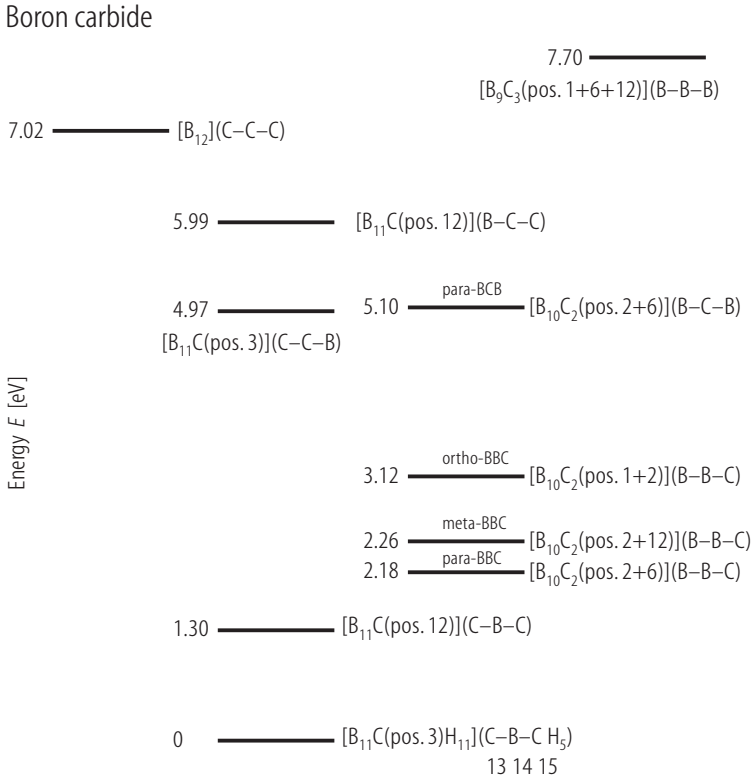

Fig. 7.

Boron carbide, hypothetical B_{12}(CBC). Total and component densities of states for idealized structure B_{12}(CBC). Top panel: total density of states per unit cell; lower panels: component densities of states per atom. The Fermi energy is shown at 0.0 eV [90S].

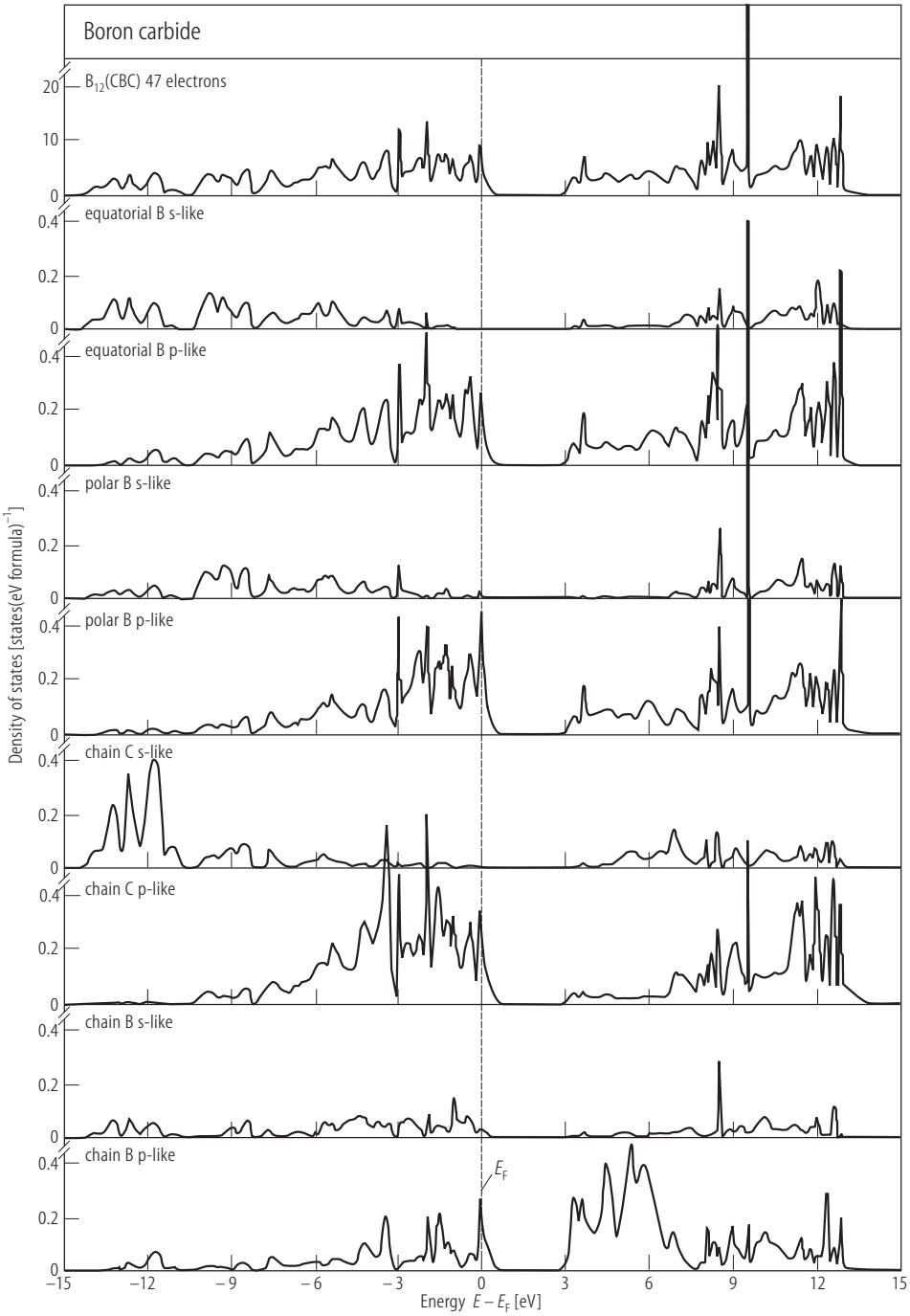

Fig. 8.

Boron carbide. Density of hopping sites vs. C content, (open triangles) derived from dc conductivity according to Mott's law for variable-range hopping and (full circles) $A^{1/2}$ (derived from the dynamical conductivity in the FIR range according to $\sigma(\omega) = A\int_0^\infty [x^4 / (e^x + i(\omega_\tau / \omega))]dx$ with $A \propto n_s^{2} \cdot T$ (n_s, density of hopping states), ω_τ, relaxation frequency; open circles, density of B_{12} icosahedra for comparison [97S, 98W].

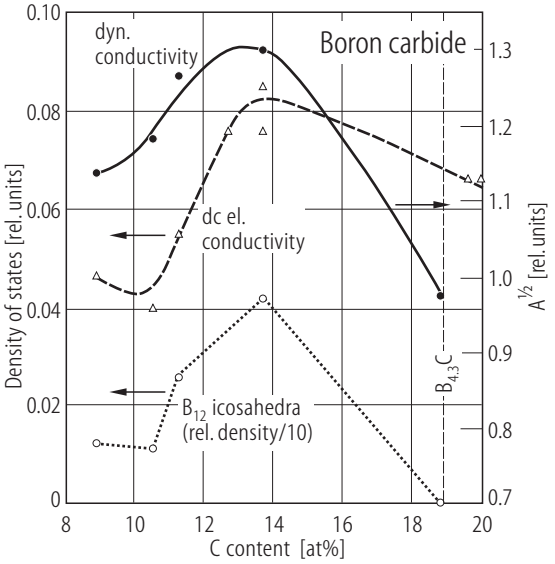

Fig. 9.

Boron carbide. Contours of constant charge density in the surface of $B_{11}C$ (CBC) icosahedron. a, b, polar B (neighbored to the polar C); c, polar C; d, k, v, equatorial B (neighbored to the polar B); g, h, w, equatorial B (neighbored to the polar C); x, y, z, polar B (separated from polar C) [90B1]. Values at the contours in millielectrons per cubic bohr.

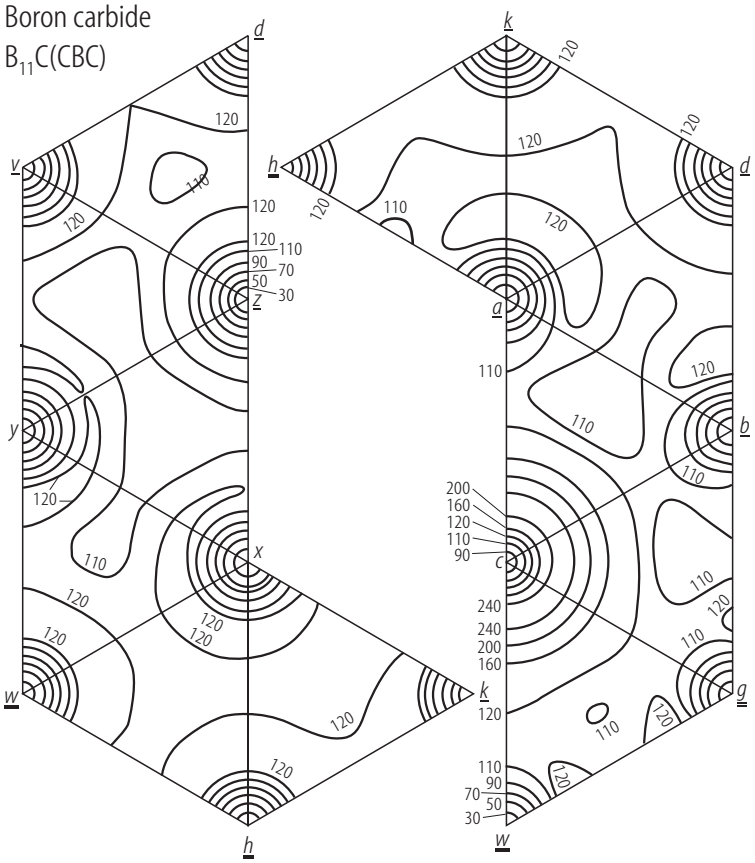

Fig. 10.

Al_3BC_3. XANES spectrum compared with those of some other boron compounds (boron carbide, B_2O_3, hexagonal BN) [98M].

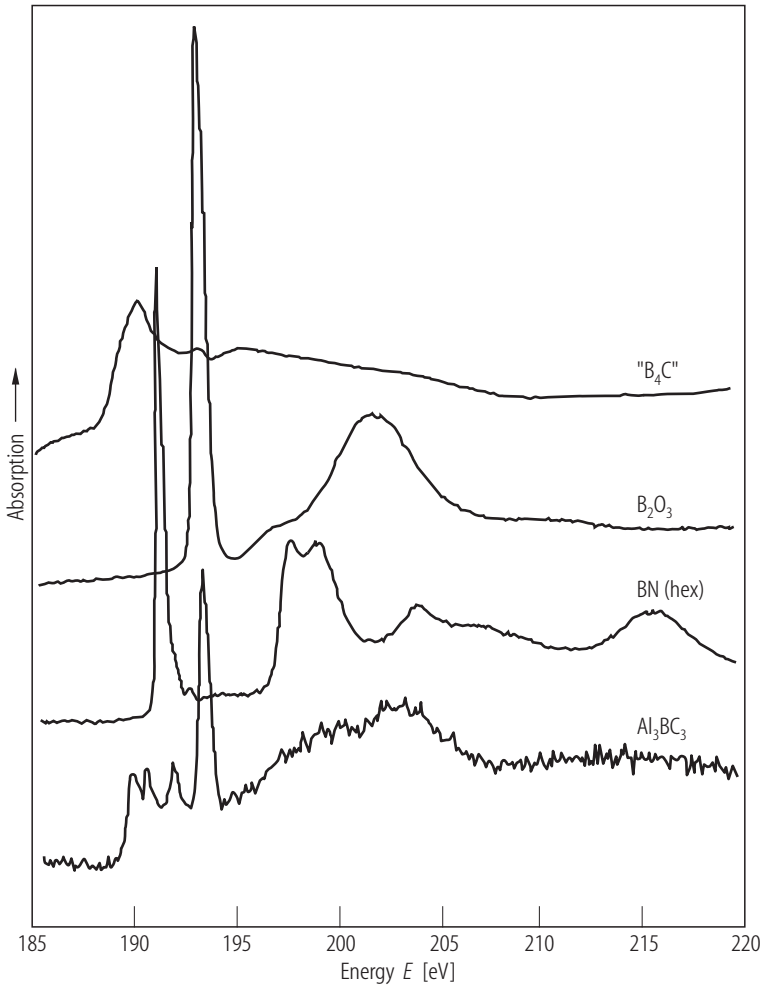

Fig. 11.

Boron carbide. B-KVV and C-KVV Auger lines in the derivative mode for (*a*) fracture surface of commercial B_4C; (*b*) IB cleaned B_4C surface; (*c*) IB cleaned B_9C surface; (*d*) boron-rich region of B_9C fracture surface; (*e*) carbon-rich region of B_9C fracture surface [86M].

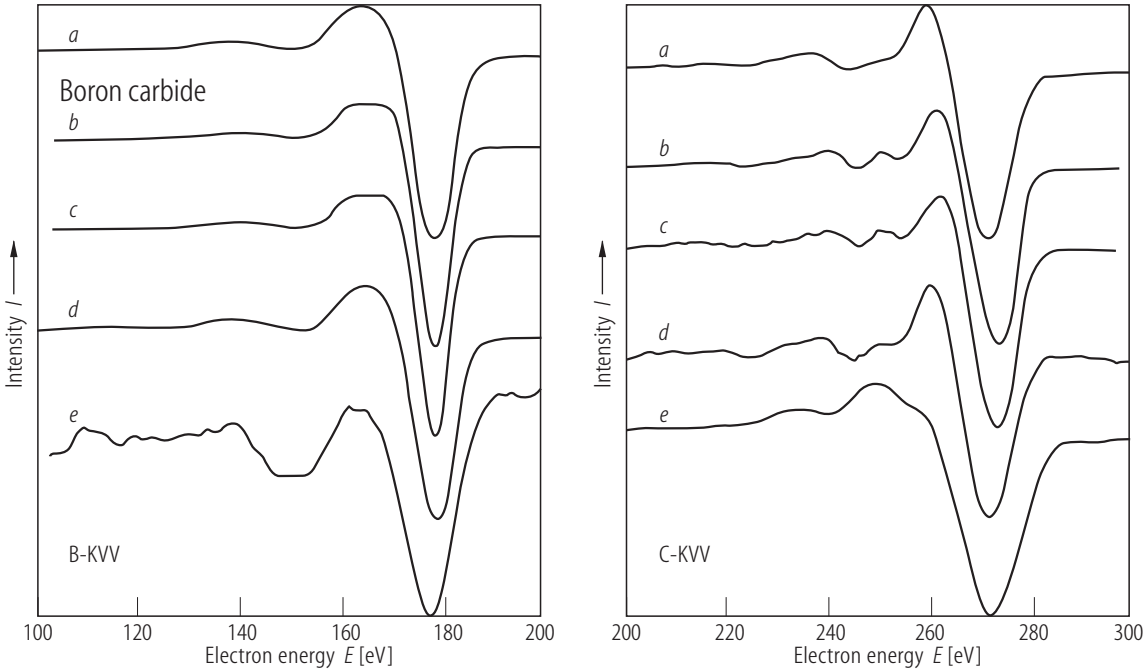

Fig. 12.

Boron carbide (B_4C, B_9C). Electrical conductivity vs. pressure [85S].

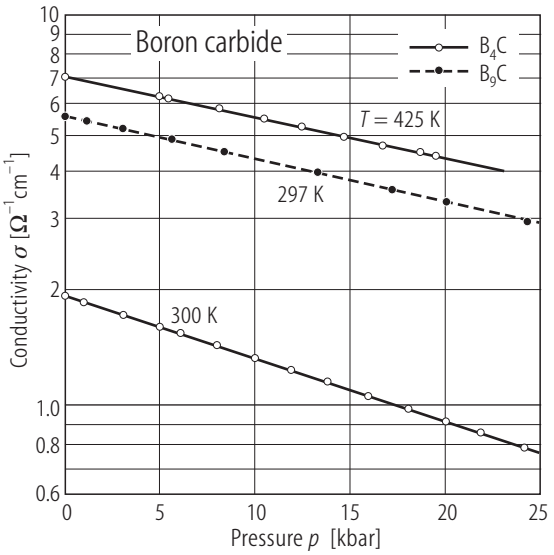

Fig. 13.

Boron carbide. (unknown composition; approximately $B_{12}C_3$, polycrystalline samples). Absorption coefficient vs. wavelength [71W, 74W].

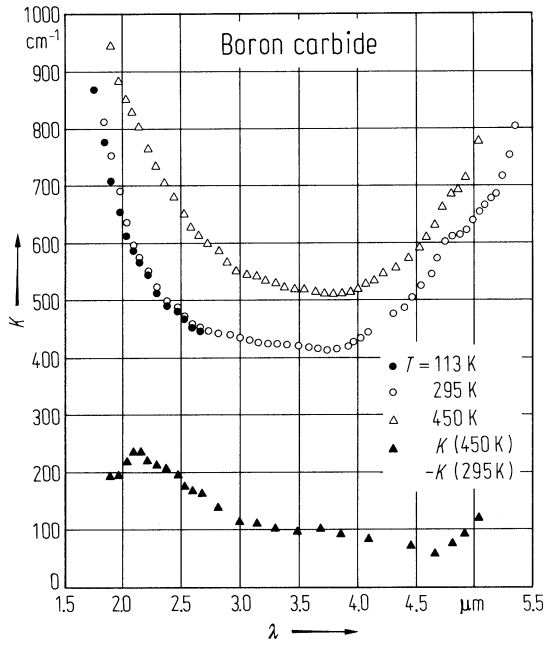

Fig. 14.

Boron carbide ($B_{4.3}C$). Photoluminescence spectrum of $B_{4.3}C$ (exact sample composition $B_{4.23}C$) at 290K. Excitation with the 514.5 nm (2.4 eV) line of an Ar Laser; intensity 280 mW/mm^2. Circles, experimental results, thin solid line, averaged experimental results, bold solid line, recombination model of free excitons; dashed line, model for the transition of electrons between energy band and defect level [99S2].

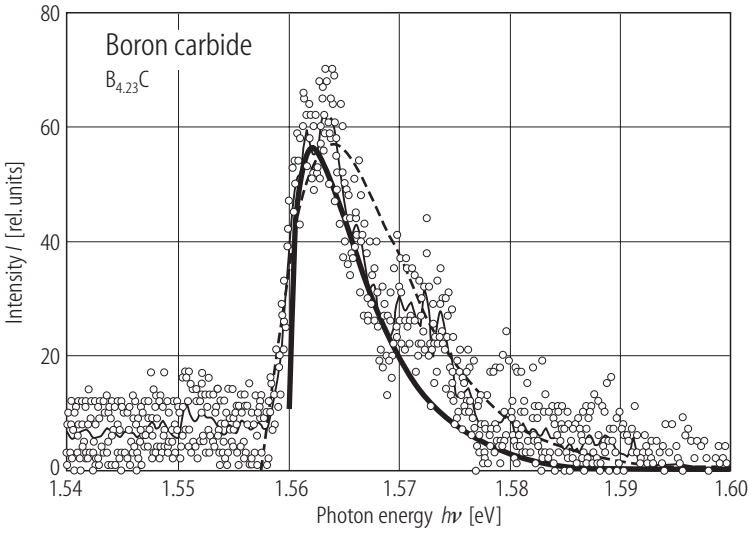

Fig. 15.

Boron carbide. Preliminary band scheme, which is compatible with the experimentally determined transition energies. The donor level has not yet been experimentally proved [98S, 99S1]. Energy values relative to the valence band edge for $B_{4.3}C$ at T = 300 K.

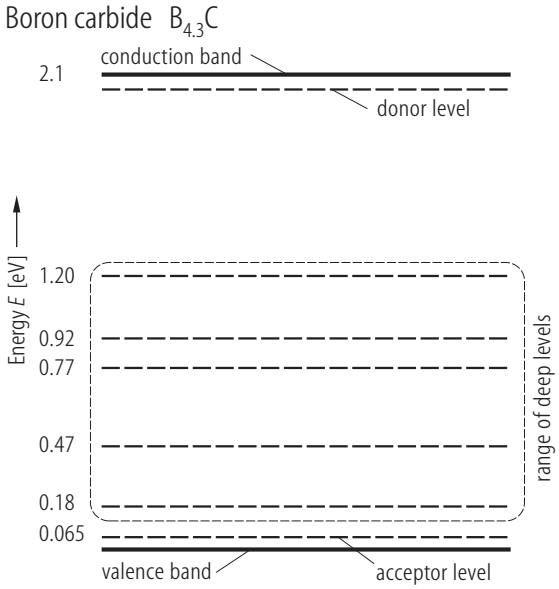

Fig. 16.

Boron carbide. Thermal activation energies of the electrical conductivity of boron carbide vs. C content; full circles, estimated from published diagrams [86W1, 86W4], open circles [86W2, 91W1].

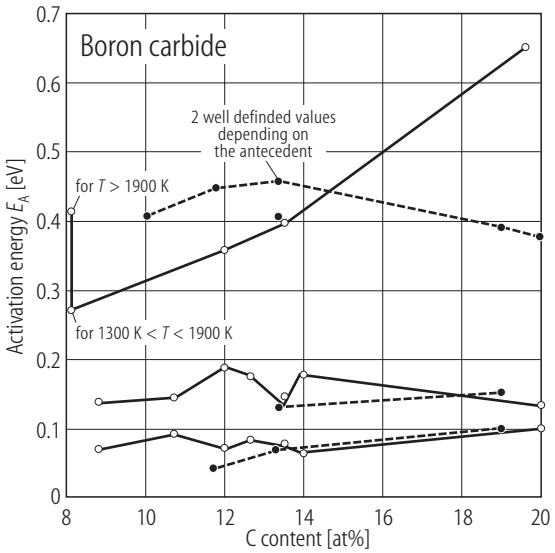

Fig. 17.

Boron carbide. Activation energy of the electrical conductivity of boron carbide of different composition vs. reciprocal temperature [80W1, 81W2]. (Sample compositions: 1) $B_{12.94}C_{2.06}$; 2) $B_{12.35}C_{2.65}$; 3) $B_{12.28}C_{2.72}$; 4) $B_{12.13}C_{2.87}$; 5) $B_{12.01}C_{2.99}$; 6) $B_{10.6}C_{4.41}$; 7, 8) [70G] unknown composition, accordingly analyzed measurements.).

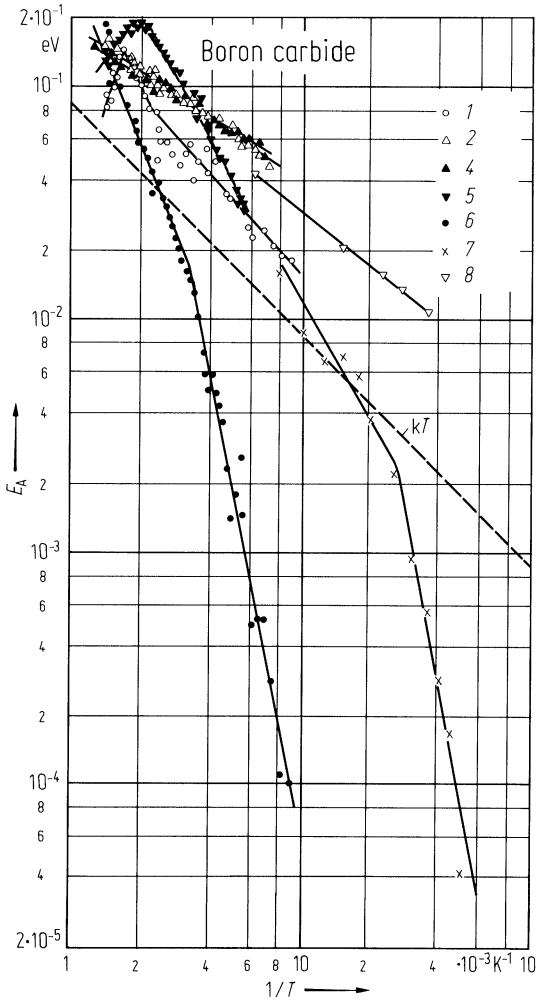

Fig. 18.

Boron carbide :N. **(a)** Rutherford backscattering spectra of nitrogen-implanted and unimplanted boron carbide and **(b)** their difference showing the implantation profile [91R]. Nominal composition is B_4C, probably close to the carbon-rich limit of the homogeneity range $B_{4.3}C$.

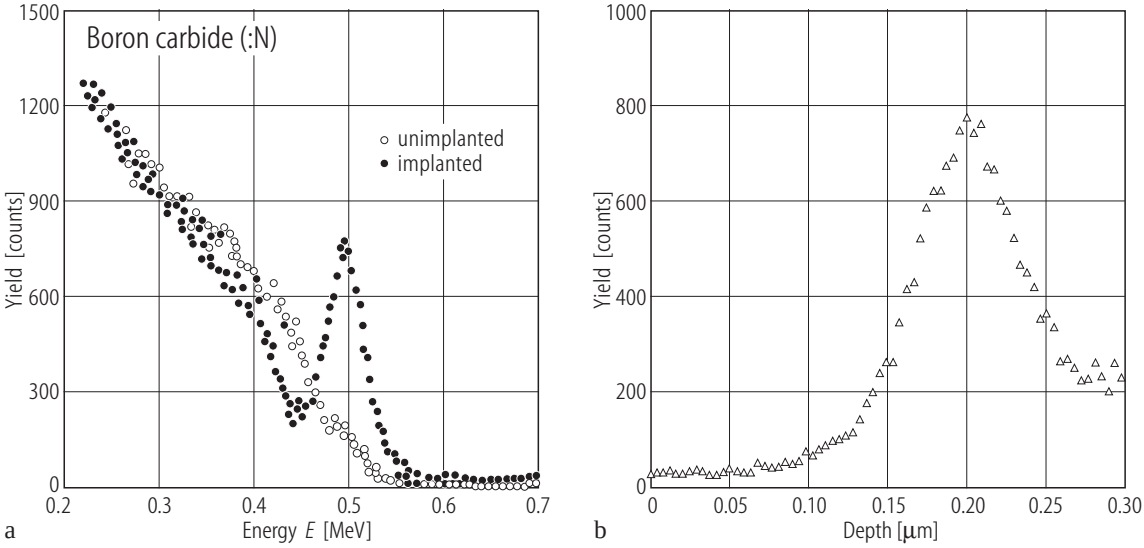

Fig. 19.

$^{10}B_{4.3}C$. Second derivatives of the real and the imaginary parts of the dielectric function [97W].

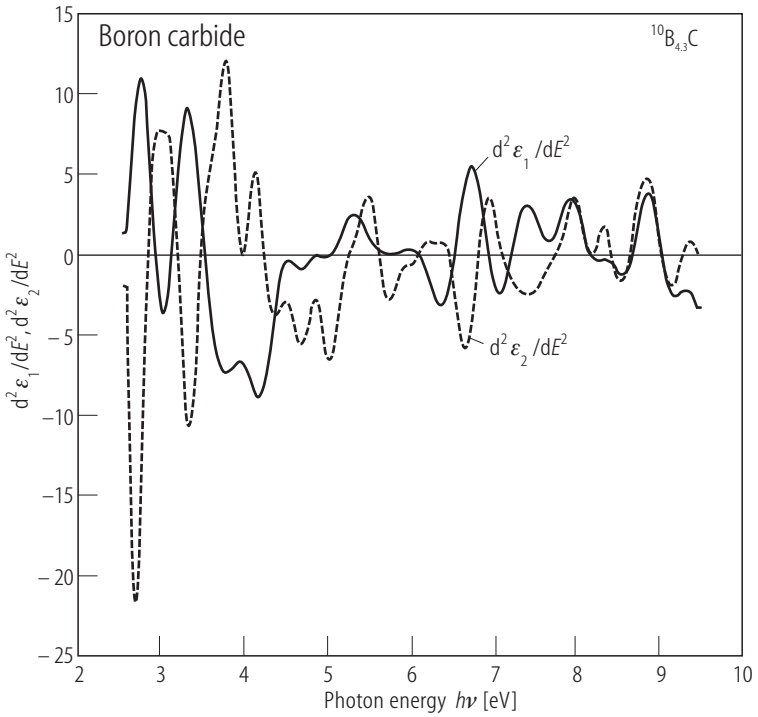

Fig. 20.

Boron carbide. ESR spectrum of boron carbide with 18 at.% C at 150 K [96C].

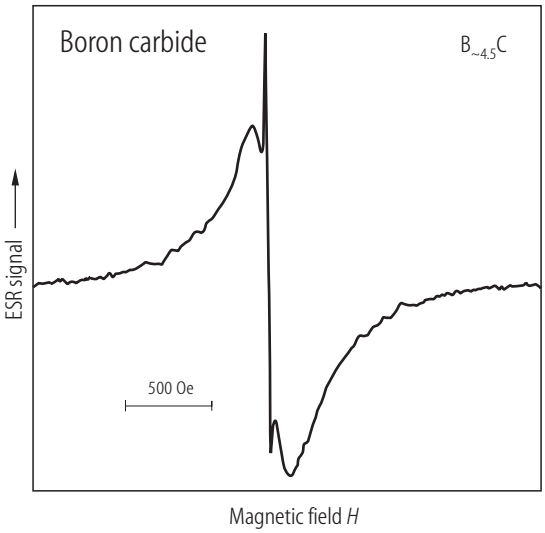

Fig. 21.

Boron carbide. ESR results. **(a)** Spin density/cell, **(b)** susceptibility (in CGS-emu), **(c)** *g*-factor, **(d)** linewidth of boron carbide with high carbon concentration (> 19 at.%) vs. *T* [96C].

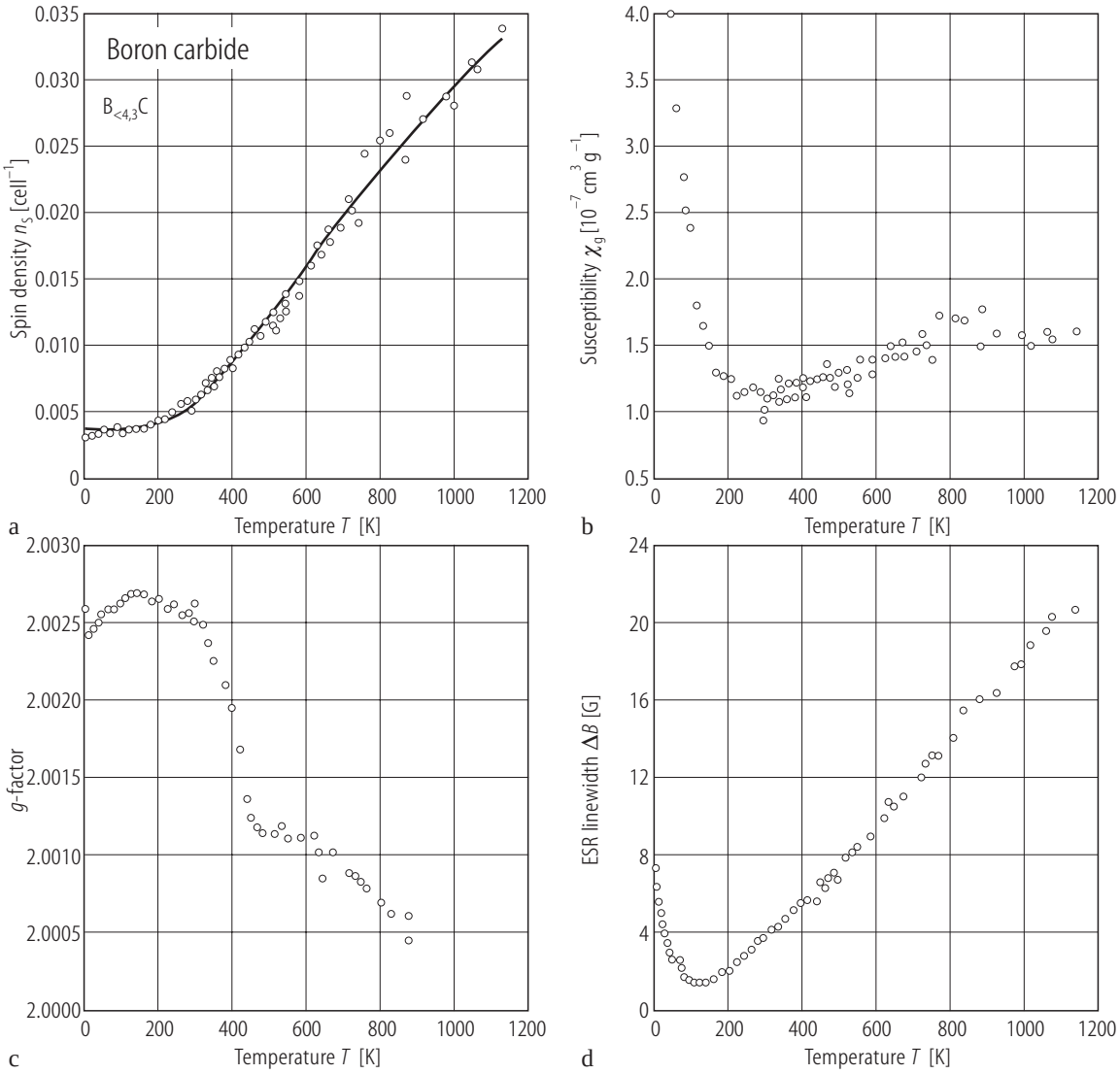

Fig. 22.

Boron carbide. ESR spin densities of boron carbide with **(a)** 18.2 and **(b)**16 at.% C, respectively compared with the Hall density $n_H=1/eR_H$ vs. T [96C].

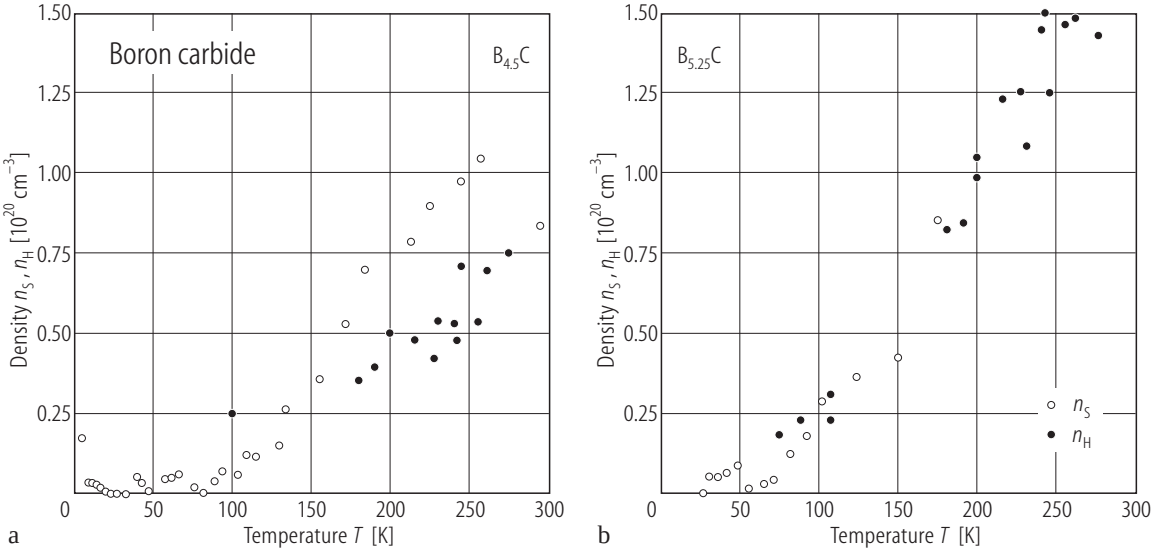

Fig. 23.

Boron carbide ($B_{4.3}C$). Spin density n_s of $B_{4.3}C$ [96C] with fit [98S] compared with the Hall density $n_H=1/|eR_H|$ of $B_{8.1}C$ and $B_{4.1}C$ [90W3]. The fit according to the equation $n_s = (N_0–n_0)+ n_0 \exp(–E_A/k_BT)$ (N_0, whole density of acceptor states; n_0, density of occupied acceptor states; E_A, energetical distance to the next unoccupied level) is based on $(N_0–n_0) = 1.3\cdot10^{19}$ cm$^{–3}$, $n_0 = 2.6\cdot10^{20}$ cm$^{–3}$ (compensation ~ 95 %), E_A = 100 meV. (see Fig. 15).

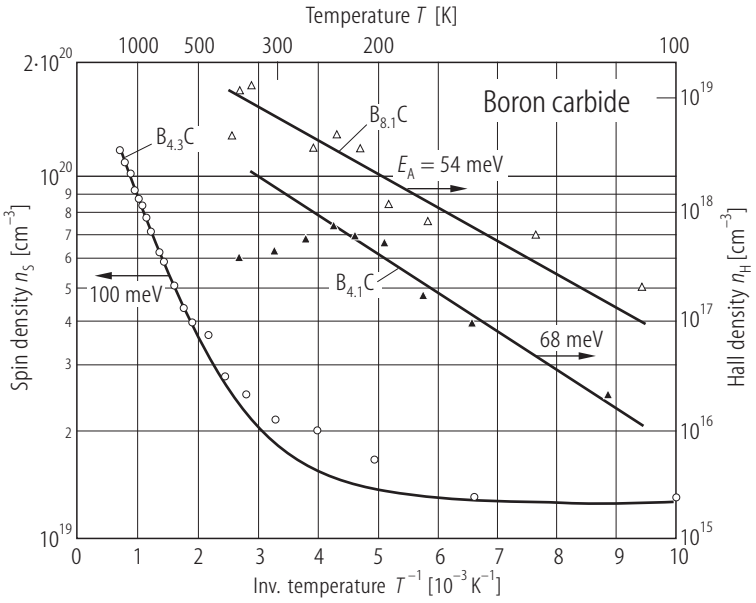

Fig. 24.

Boron carbide. Magnetic susceptibility **(a)** and ESR linewidth **(b)** of boron carbide with 18, 16, 13 and 10 at.% C vs. *T* [96C]. "Single crystal" with a composition close to the carbon-rich homogeneity limit, precipitated from a metallic copper solvent by slowing cooling from 2000 to 1300 K.

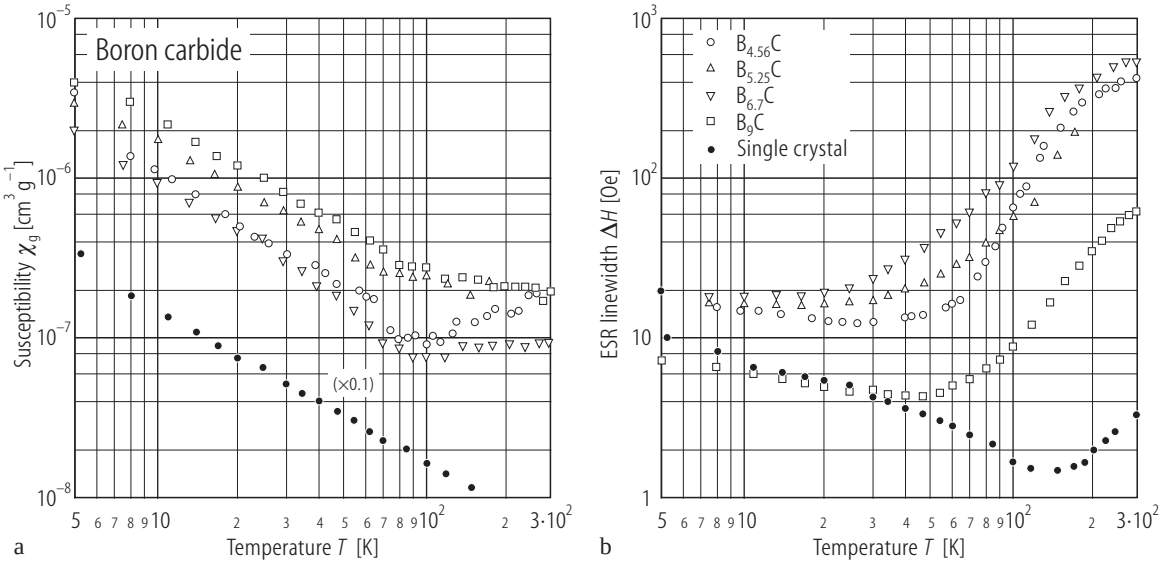

Fig. 25.

Boron carbide. ESR linewidth (triangles) compared to that of the Hall mobility (circles). solid symbols: 16 at.% C, open symbols: 18.2 at.% C [96C].

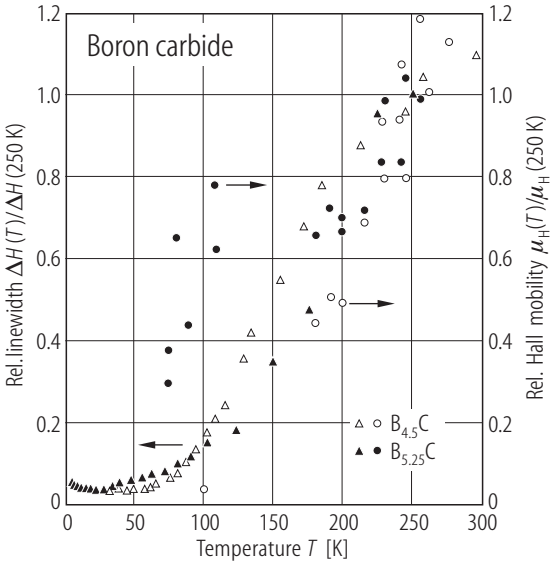

Fig. 26.

Boron carbide. ESR spin susceptibility vs. *T* for (open triangles) polycrystal (ESK, Elektroschmelzwerk Kempten), (open circles) single crystal (ESK, Elektroschmelzwerk Kempten), (full circles) hot-pressed (Eagle-Picher), (full triangles down) hot-pressed (GA Technologies) [87V].

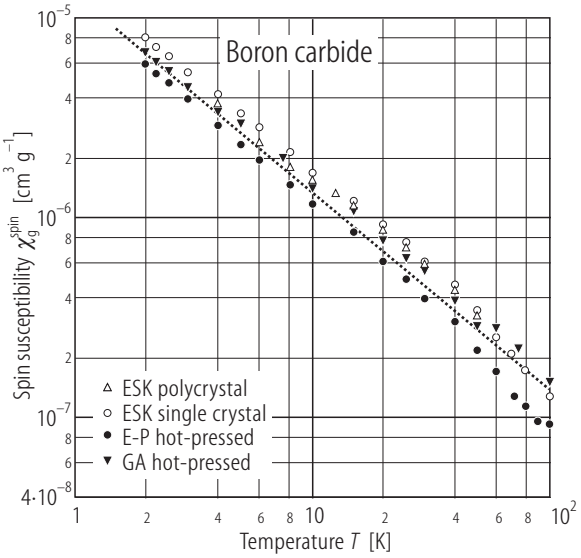

Fig. 27.

Boron carbide. ESR linewidth at 4K vs. arbitrary magnetic field orientation for (open circles) single crystal, (full circles) hot-pressed ceramic sample (cp. Fig. 26) [87V].

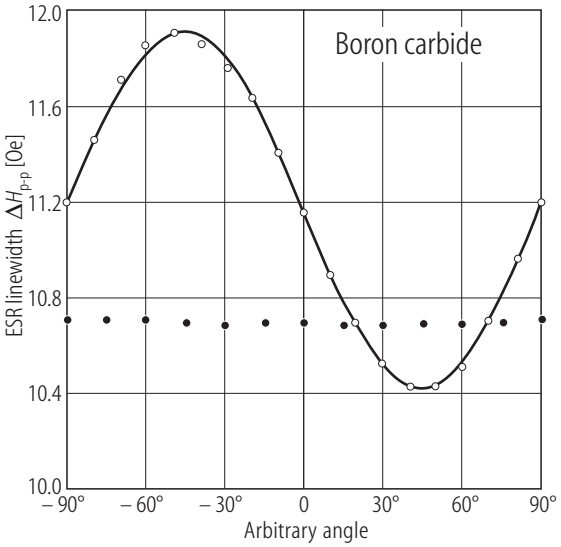

Fig. 28.

Boron-carbon system. FPR results of powders (particle size < 50 μm) [80V]. a) relative line intensity vs. C content. b) line width vs. C content. Data of different samples.

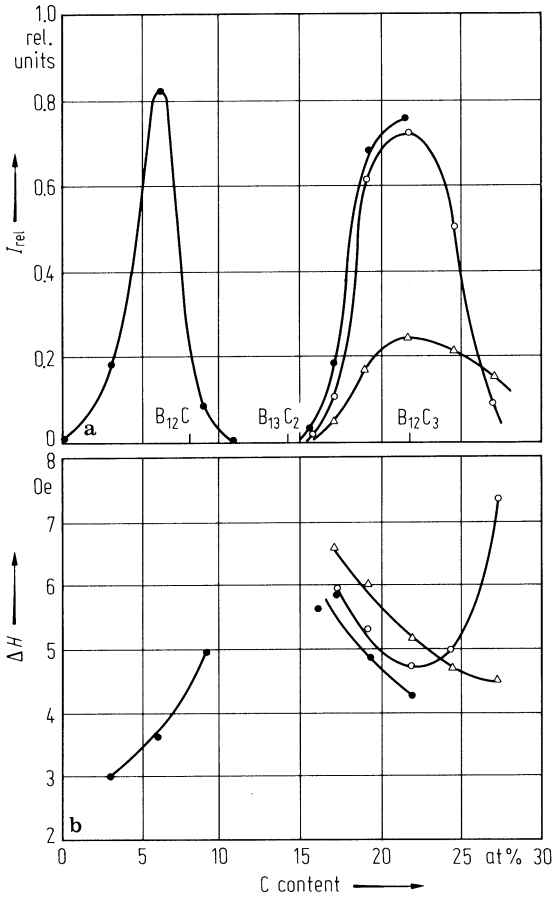

Fig. 29.

Boron carbide. Brillouin zone (rhombohedral lattice) [81A2, 83A1].

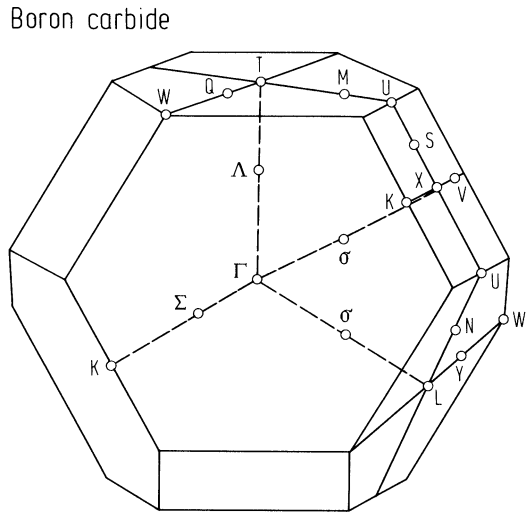

Fig. 30.

Boron carbide. Valence electron density distribution in the B(3), C, B(1), B(2) plane (B(1) and B(2) are icosahedral atoms, B(3) and C are atoms of the C–B–C chain. Levels are at 0.1 eÅ^{-3}, negative contours are dotted [79K2].

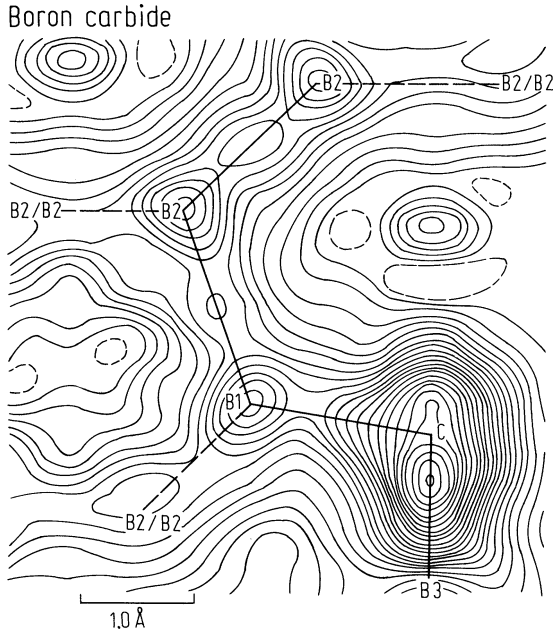

Fig. 31.

Boron carbide. Distance between the Fermi level and the valence band edge respectively the mobility edge vs. the medium distance R of the C atoms [80W1; 81W2]. A possible contribution of a thermally activated mobility is included into the energy scale. $R = \{(4\pi/3)N\}^{1/3}$ where N is the number of C atoms per cm^3.

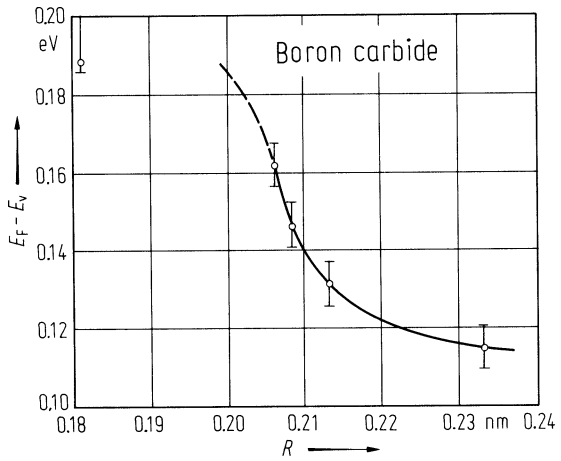

Fig. 32.

Boron carbide. Derivatives of the density of states g(E) and of the hopping energy W at the Fermi level vs. the shift of the Fermi level relative to the valence band edge E (resp. the mobility edge). This shift includes that the C content affects the density of states and the occupation density as well [80W1, 81W2].